A METHOD OF LQR USING VELOCITY CONTROL FOR UNICYCLE ROBOT

Thi-Ai-Van Nguyen, Dinh-Hau Vu, Ha-Gia-Huy Nguyen, Nguyen-Chi-Nghia Pham, Khanh-Hoang Cao, Thanh-An Vo, Hong-Long Le, Minh-Tam Nguyen *

Ho Chi Minh City University of Technology and Education (HCMUTE)
01, Vo Van Ngan Str, Thu Duc city, Ho Chi Minh City, Vietnam
***** Corresponding author. E-mail: tamnm@hcmute.edu.vn

Abstract: This study explores the use of Linear Quadratic Regulator (LQR) control to stabilize a unicycle robot, a key example within the unicycle-type mobile robot category. Despite its inherent instability, the unicycle robot offers notable advantages over multi-wheeled, statically stable designs, including reduced spatial requirements due to its single ground contact point. The system is modeled using two axes: the roll axis, represented as an inverted pendulum managed by the wheel, and the pitch axis, modeled as a reaction wheel inverted pendulum controlled by a reaction disk. LQR is recognized as an effective approach for controller design in nonlinear systems. This research focuses on designing, implementing, and evaluating LQR controllers with varying weighting matrices to analyze their influence on system performance. Comparative case studies are conducted by altering the weighting matrices and benchmarking the results against the initial configuration. Experimental outcomes highlight the potential of LQR control for achieving robust stabilization of unicycle robots.
Keywords: unicycle robot, velocity control, LQR control, speed control.

1. Introduction

Unicycle robots were initially introduced in [1], where mathematical equations were derived, and the model's controllability was evaluated. Later, in [2], the design of a unicycle robot was inspired by the concept of a person pedaling a wheel. Although this study presented mathematical equations for balancing the robot without using a controller, the model remained unstable and overly complex. Despite these limitations, it led to further advancements, such as Honda's creation of the UX-3 personal vehicle and Murata Manufacturing's development of the Murata Girl. In [3], new dynamic equations were introduced by splitting the robot into two parts: the upper reaction wheel pendulum and the lower inverted pendulum, which were decoupled. Intelligent algorithms, like fuzzy logic, were applied to each part, but high-speed movements increased balancing time and adaptability. Studies [4-5] explored dynamic control for the single-wheel robot's roll and pitch axes, utilizing robust control for roll and linear control for pitch, though some output chatter persisted despite efforts to reduce it using a sign function. A new single-wheel model with active omnidirectional wheels was introduced in [6], though mechanical limitations remained.

To address the equilibrium time issues in [3] and the chatter problems in [4-5], we applied a linear controller using a velocity control method. Building on the kinematic analysis and linear controller design from [10], this paper provides experimental evaluations comparing the new method with previous results for the single-wheel robot. A linear quadratic regulator (LQR) was developed for the roll and pitch axes, with a focus on finding appropriate matrix values. These values were fine-tuned and verified through experiments, showing that the linear controller is effective for this model when using velocity control. Additionally, the calibration process was consistent with the theoretical framework presented in [8-9].

2. Dynamic

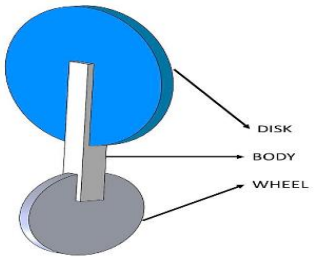

Fig. 1. A simple depiction of the unicycle robot model.

In this section, we analyze the functioning of the unicycle robot. The model is split into two separate bodies for the pitch and roll axes: the pitch axis is represented by an inverted pendulum, while the roll axis is modeled as a reaction wheel-balanced inverted pendulum. The dynamic equations for both axes were derived using the Lagrange method. Figure 1 shows the constructed unicycle robot, which is composed of three primary parts: a rotating disk, the robot body, and a rotating wheel, with their respective masses labeled as m_D, m_B, m_W.

2.1. Dynamic Model of the Roll Axis

The roll axis dynamics are based on the model of a reaction wheel inverted pendulum, which includes two main components: a disk and a body compound wheel, collectively called the bottom body. **Fig. 2** shows the robot's axes used for calculating dynamic roll. The symbols l and l_G represent the distances from the ground to the center of the disk and the center of gravity of the bottom body, respectively. r_D and ϕ_D correspond to the disk's radius and its rotation angle, while ϕ refers to the rotation angle of the robot in the roll direction. The masses of the bottom body, robot body, and disk are denoted by m_{BW}, m_B, m_D, respectively. Two position vectors, $\vec{r}_1, \vec{r}_2$ are defined to calculate the Lagrangian for the robot: one vector points from the coordinate origin to the disk's center, and the other to the center of the bottom body.

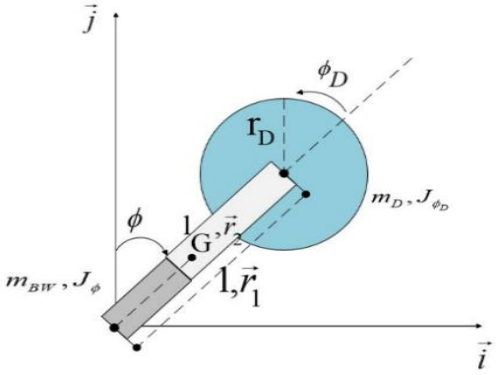

Fig. 2. Model of the unicycle robot for the roll axis

$$\begin{aligned}\vec{r}_1 &= l_G \sin(\phi)\vec{i} + l_G \cos(\phi)\vec{j} \\ \vec{r}_2 &= l \sin(\phi)\vec{i} + l \cos(\phi)\vec{j}\end{aligned} \tag{1}$$

From Section 2.1 of [10], we obtain the following formula:

$$\begin{aligned}\alpha v_R &= (J_\phi + l^2{}_G m + l^2 m_D)\ddot{\phi} \\ &\quad - g(l_G m + l m_D)\phi - \beta(\dot{\phi} - \dot{\phi}_D) \\ -\alpha v_R &= J_{\phi_D}(\ddot{\phi}_D + \ddot{\phi}) + \beta(\dot{\phi} - \dot{\phi}_D)\end{aligned} \tag{2}$$

With $\alpha = nKt / R_m, \beta = \alpha + f_m$

2.2. Dynamic Model of the Pitch Axis

The pitch axis dynamics are based on an inverted pendulum model, which comprises two main components: a wheel and a compound disk representing the body, collectively known as the upper body. Figure 3 shows the robot's axes used for calculating pitch dynamics. L denotes the distance from the center of the wheel to the center of the upper body. R_W is the radius of the wheel, while θ_W and θ represent the rotation angles of the wheel and the pitch axis, respectively. The masses of the wheel and upper body are indicated m_W and m_{BD} respectively. Two position vectors, $\vec{r}_1$ and $\vec{r}_2$ are defined to compute the Lagrangian for the robot, representing vectors from the coordinate origin to the centers of the wheel and the upper body.

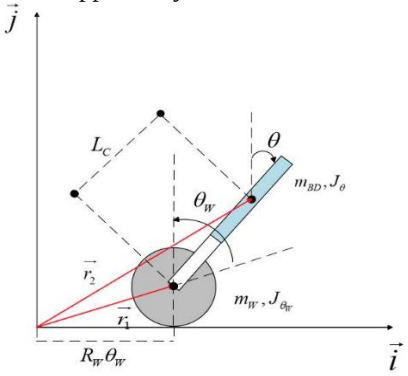

Fig. 3. Model of the unicycle robot for the pitch axis

$$\begin{aligned}\vec{r}_1 &= R_W\theta_W\vec{i} + R_W\vec{j} \\ \vec{r}_2 &= (R_W\phi + L_C \sin\theta)\vec{i} + (R_W + L_C\cos\theta)\vec{j}\end{aligned} \tag{3}$$

According to Section 2.2 of [10], the following formula is derived:

$$\begin{aligned}\alpha v_P &= \left(J_{\theta_W} + J_m n^2 + (m_W + m_{BD})R^2{}_W\right)\ddot{\theta}_W \\ &\quad + \left(L_C m_{BD} R_W - J_m n^2\right)\ddot{\theta} - \beta\dot{\theta} + \beta\dot{\theta}_W \\ -\alpha v_P &= (L_C m_{BD} R_W - J_m n^2)\ddot{\theta}_W - \beta\dot{\theta}_W + \beta\dot{\theta} \\ &\quad + \left(J_\psi + L_C{}^2 m_{BD} + J_m n^2\right)\ddot{\theta} - g L_C m_{BD}\theta\end{aligned} \tag{4}$$

3. Design LQR Controller Using Velocity Control

3.1. LQR for Roll Axis

Based on the matrices $\mathbf{Q}, \mathbf{R}$ provided in Section 4.1 of reference [10], we derive:

$$\mathbf{Q} = \begin{bmatrix} Q_1 & 0 & 0 \\ 0 & Q_2 & 0 \\ 0 & 0 & Q_3 \end{bmatrix}; \mathbf{R} = [R_1] \tag{5}$$

The coefficients Q_1, Q_2, Q_3 reflect the weight assigned to the state variables x_1, x_2, x_3. Increasing any of these coefficients will make the corresponding variable more responsive compared to the others. However, this change could stabilize the system while potentially leading to the robot losing its balance. Hence, careful selection of the matrix $\mathbf{Q}$ is crucial. The matrix $\mathbf{R}$ indicates the priority given to the input v_R .

The matrices $\mathbf{Q}$ and $\mathbf{R}$ were selected with the following values:

$$\mathbf{Q}=\begin{bmatrix}250 & 0 & 0\\ 0 & 100 & 0\\ 0 & 0 & 100\end{bmatrix};\mathbf{R}=[R_1]=1 \quad (6)$$

The optimal gain can be calculated as outlined in [8] and [9] as follows:

$$K=\begin{bmatrix}-459.7259 & -137.9285 & -10.4870\end{bmatrix} \quad (7)$$

The control input is expressed as:

$$v_R=-Kx \quad (8)$$

where $x=\begin{bmatrix}x_1 & x_2 & x_3\end{bmatrix}^T=\begin{bmatrix}\phi & \dot{\phi} & \dot{\phi}_D\end{bmatrix}^T$

3.2. LQR for Pitch Axis

Based on the matrices $\mathbf{Q},\mathbf{R}$ provided in Section 4.2 of reference [10], we derive:

$$\mathbf{Q}=\begin{bmatrix}Q_4 & 0 & 0\\ 0 & Q_5 & 0\\ 0 & 0 & Q_6\end{bmatrix};\mathbf{R}=[R_2] \quad (9)$$

The matrices $\mathbf{Q}$ and $\mathbf{R}$ were selected with the following values:

$$\mathbf{Q}=\begin{bmatrix}250 & 0 & 0\\ 0 & 100 & 0\\ 0 & 0 & 100\end{bmatrix};\mathbf{R}=[R_2]=1 \quad (10)$$

Thus, the matrix K is obtained as follows:

$$K=\begin{bmatrix}278.70 & 716.00 & 9.50\end{bmatrix} \quad (11)$$

The control input is expressed as:

$$v_P=-Kx \quad (12)$$

Where $x=\begin{bmatrix}x_4 & x_5 & x_6\end{bmatrix}^T=\begin{bmatrix}\theta_W & \dot{\theta}_W & \dot{\theta}\end{bmatrix}^T$

4. Simulation

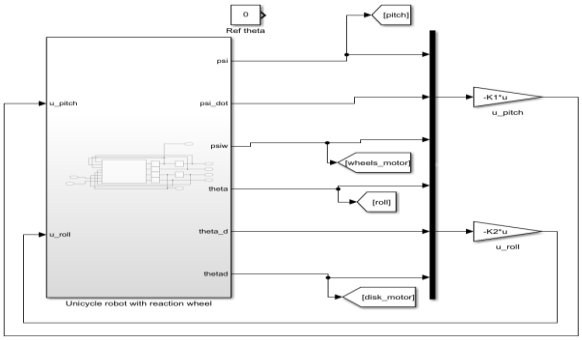

Fig. 4. Diagram of the unicycle robot simulation using an LQR controller

4.1. Standard LQR

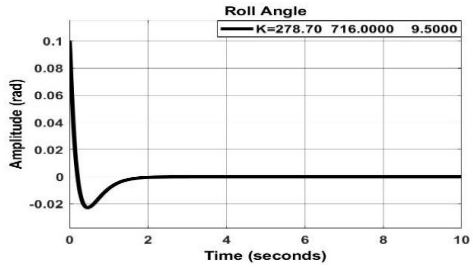

Fig. 5. Stabilized LQR value for Roll axis

$$\mathbf{Q}=\begin{bmatrix}250 & 0 & 0\\ 0 & 100 & 0\\ 0 & 0 & 100\end{bmatrix}$$

$$\rightarrow K=\begin{bmatrix}278.70 & 716.00 & 9.50\end{bmatrix}$$

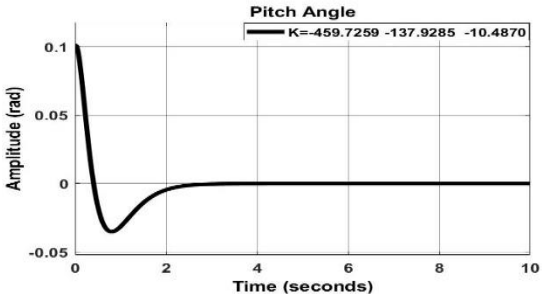

Fig. 6. Stabilized LQR value for Pitch axis

$$\mathbf{Q}=\begin{bmatrix}250 & 0 & 0\\ 0 & 100 & 0\\ 0 & 0 & 100\end{bmatrix}$$

$$\rightarrow K=\begin{bmatrix}-459.7259 & -137.9285 & -10.4870\end{bmatrix}$$

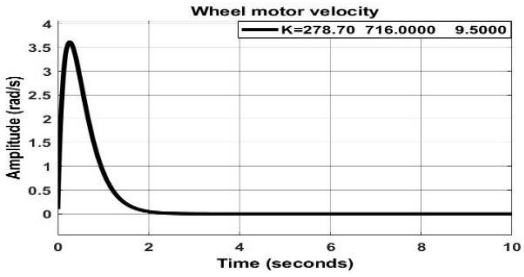

Fig. 7. Output result of the wheel motor velocity

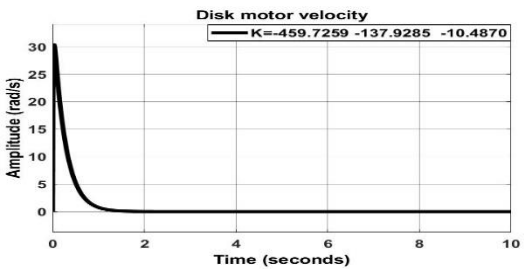

Fig. 8. Output result of the disk motor velocity

Comment:

- With the standard values, we can see that the roll angle changes from 0.1 rad to -0.02 rad over about 1.5 seconds, and then stabilizes at the equilibrium position. Similarly, the pitch angle stabilizes at 0 after 2 seconds. Therefore, the velocity of the wheel and disk motors reaches equilibrium at 2 seconds and in the first 1 second, respectively.

4.2. Change Q_1 and Q_4 value

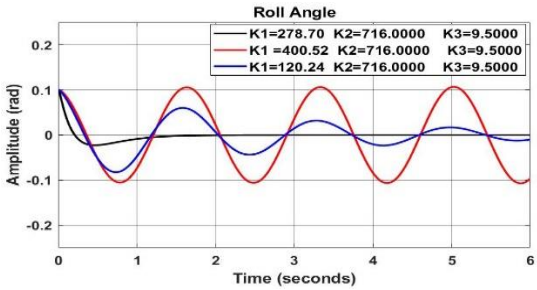

Fig. 9. The result modifies the Q_1 value for Roll axis.

- Increase Q_1 value:

$$\mathbf{Q} = \begin{bmatrix} 450 & 0 & 0 \\ 0 & 100 & 0 \\ 0 & 0 & 100 \end{bmatrix}$$

$$\rightarrow K = \begin{bmatrix} -652.7259 & -137.9285 & -10.4870 \end{bmatrix}$$

- Decrease Q_1 value:

$$\mathbf{Q} = \begin{bmatrix} 100 & 0 & 0 \\ 0 & 100 & 0 \\ 0 & 0 & 100 \end{bmatrix}$$

$$\rightarrow K = \begin{bmatrix} -252.5567 & -137.9285 & -10.4870 \end{bmatrix}$$

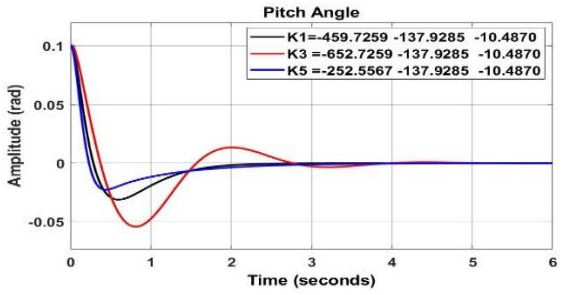

Fig. 10. The result modifies the Q_4 value for Pitch axis.

- Increase Q_4 value:

$$\mathbf{Q} = \begin{bmatrix} 550 & 0 & 0 \\ 0 & 100 & 0 \\ 0 & 0 & 100 \end{bmatrix}$$

$$\rightarrow K = \begin{bmatrix} 400.52 & 716.00 & 9.50 \end{bmatrix}$$

- Decrease Q_4 value:

$$\mathbf{Q} = \begin{bmatrix} 150 & 0 & 0 \\ 0 & 100 & 0 \\ 0 & 0 & 100 \end{bmatrix}$$

$$\rightarrow K = \begin{bmatrix} 120.24 & 716.00 & 9.50 \end{bmatrix}$$

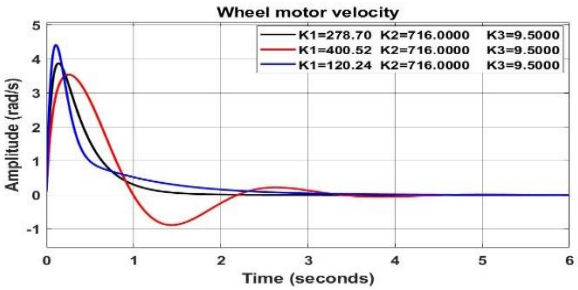

Fig. 11. Output result of the wheel motor velocity

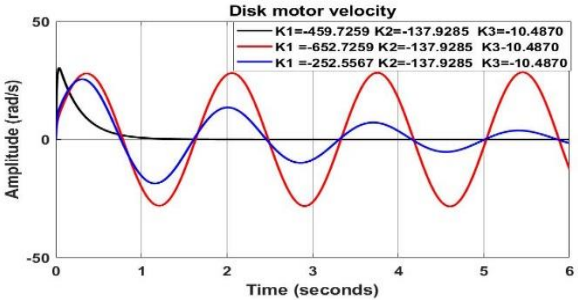

Fig. 12 Output result of the disk motor velocity

Comment:

- When increasing Q_1, the roll angle oscillates with an amplitude from 0.1 rad to -0.1 rad, with a period of 1.5 seconds. The wheel motor velocity takes longer to stabilize—about 4 seconds.
- When decreasing Q_1, the roll angle tends to gradually reduce the oscillation amplitude to 0 at t = 10 seconds. The wheel motor velocity overshoots to 4.5 rad and decreases to 0 at 3 seconds.
- When increasing Q_4, the pitch angle starts at 0.1 rad and quickly decreases to -0.05 rad within 1 second, reaching equilibrium at 0 by 4 seconds. The disk motor velocity oscillates with an amplitude of [-25; 25] rad, a period of 1.75 seconds, and starts at 10 rad.
- When decreasing Q_4, the pitch angle follows a pattern similar to the standard signal, and the disk motor velocity behaves similarly to the roll angle but with an inverse cycle.

Let me know if you need any changes!

4.3. Change Q_2 and Q_5 value

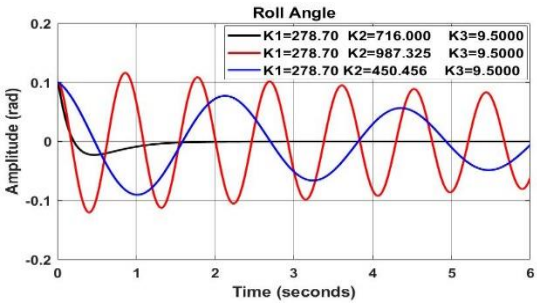

Fig. 13. The result modifies the Q_2 value for Roll axis

- Increase Q_2 value:

$$\mathbf{Q}=\begin{bmatrix}250 & 0 & 0\\ 0 & 400 & 0\\ 0 & 0 & 100\end{bmatrix}$$

$$\rightarrow K=\begin{bmatrix}-459.7259 & -350.560 & -10.4870\end{bmatrix}$$

- Decrease Q_2 value:

$$\mathbf{Q}=\begin{bmatrix}250 & 0 & 0\\ 0 & 50 & 0\\ 0 & 0 & 100\end{bmatrix}$$

$$\rightarrow K=\begin{bmatrix}-459.7259 & -82.7630 & -10.4870\end{bmatrix}$$

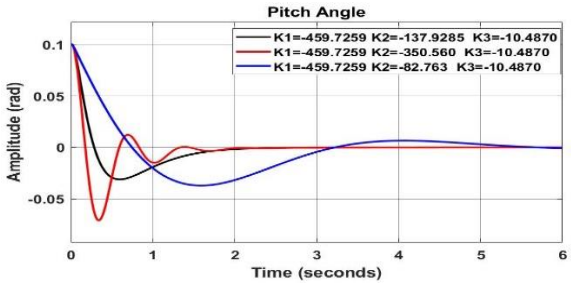

Fig. 14. The result modifies the Q_2 value for Pitch axis

- Increase Q_5 value:

$$\mathbf{Q}=\begin{bmatrix}250 & 0 & 0\\ 0 & 300 & 0\\ 0 & 0 & 100\end{bmatrix}$$

$$\rightarrow K=\begin{bmatrix}278.700 & 987.325 & 9.500\end{bmatrix}$$

- Decrease Q_5 value:

$$\mathbf{Q}=\begin{bmatrix}250 & 0 & 0\\ 0 & 30 & 0\\ 0 & 0 & 100\end{bmatrix}$$

$$\rightarrow K=\begin{bmatrix}278.700 & 450.456 & 9.500\end{bmatrix}$$

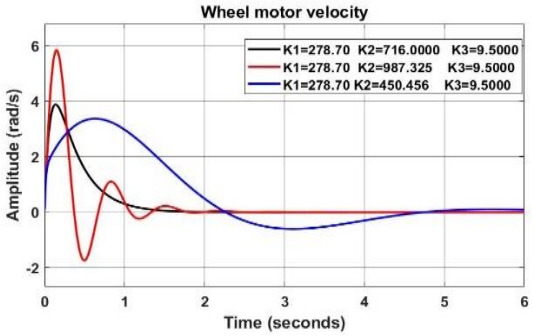

Fig. 15. Output result of the wheel motor velocity

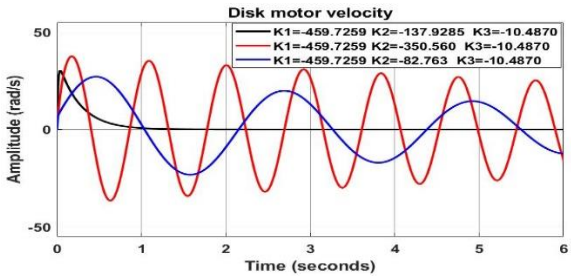

Fig. 16. Output result of the disk motor velocity

Comment:

- When increasing Q_2, the roll angle oscillates with an amplitude from 0.1 rad to -0.1 rad, with a period of 1 second. The wheel motor speed surges up to 3.5 rad within the first 0.5 seconds, then gradually decreases and stabilizes at the equilibrium position after 4 seconds.
- When decreasing Q_2, the roll angle gradually decreases with an amplitude from 0.1 rad to -0.1 rad, with a period of 2 seconds. The wheel motor speed surges up to 4.5 rad within the first 0.1 seconds, then gradually decreases and stabilizes at the equilibrium position after 3 seconds.
- When increasing Q_5, the tilt angle starts at 0.1 rad and quickly drops to -0.075 rad within 0.2 seconds, reaching equilibrium at 0 after 2 seconds. The disc motor speed oscillates with an amplitude of [-25; 25] rad, with a period of 2.5 seconds and starts at 10 rad.
- When decreasing Q_5, the tilt angle becomes unstable and tends to remain unbalanced, while the disc motor speed oscillates with a gradually decreasing amplitude from 25 rad to -25 rad, with a period of 2.5 seconds.

4.4. Change Q_3 and Q_6 value

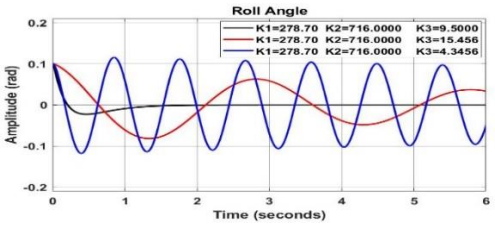

Fig. 17. The result modifies the Q_3 value for Roll axis

- Increase Q_3 value:

$$\mathbf{Q} = \begin{bmatrix} 250 & 0 & 0 \\ 0 & 100 & 0 \\ 0 & 0 & 150 \end{bmatrix}$$

$$\rightarrow K = \begin{bmatrix} -459.7259 & -137.9285 & -15.7630 \end{bmatrix}$$

- Decrease Q_3 value:

$$\mathbf{Q} = \begin{bmatrix} 250 & 0 & 0 \\ 0 & 100 & 0 \\ 0 & 0 & 40 \end{bmatrix}$$

$$\rightarrow K = \begin{bmatrix} -459.7259 & -137.9285 & -3.6532 \end{bmatrix}$$

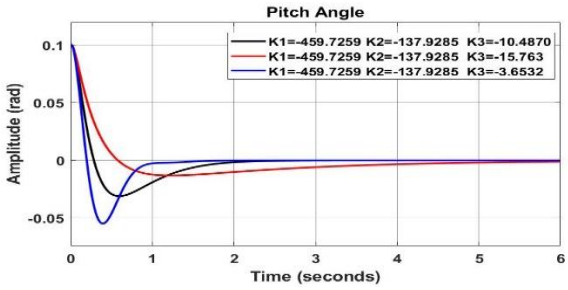

Fig. 18. The result modifies the Q_6 value for Pitch axis

- Increase Q_6 value:

$$\mathbf{Q} = \begin{bmatrix} 250 & 0 & 0 \\ 0 & 100 & 0 \\ 0 & 0 & 150 \end{bmatrix}$$

$$\rightarrow K = \begin{bmatrix} 278.70 & 716.00 & 15.456 \end{bmatrix}$$

- Decrease Q_6 value:

$$\mathbf{Q} = \begin{bmatrix} 250 & 0 & 0 \\ 0 & 100 & 0 \\ 0 & 0 & 60 \end{bmatrix}$$

$$\rightarrow K = \begin{bmatrix} 278.70 & 716.00 & 4.3456 \end{bmatrix}$$

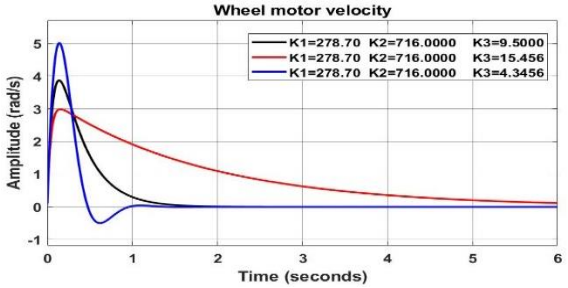

Fig. 19. Output result of the wheel motor velocity

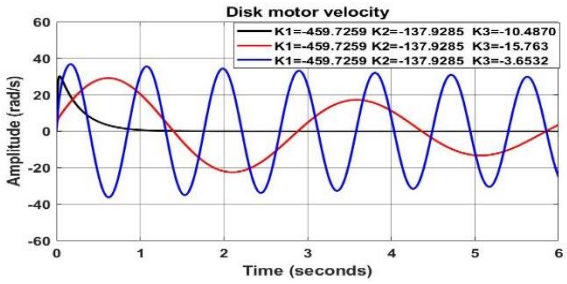

Fig. 20. Output result of the disk motor velocity

Comment:

- When increasing Q3, the roll angle oscillates with an amplitude from 0.1 rad to -0.1 rad, with a period of 1 second. The wheel motor speed surges up to 5 rad within the first 0.2 seconds, then gradually decreases and stabilizes at the equilibrium position after 1 second.
- When decreasing Q3, the roll angle gradually decreases with an amplitude from 0.1 rad to -0.1 rad, becoming unstable and tending to remain unbalanced. The wheel motor speed starts at 3 rad and then gradually decreases, approaching 0 over about 7 seconds.
- When increasing Q6, the tilt angle starts at 0.1 rad and gradually decreases to -0.02 rad, approaching 0 after 5 seconds. The disc motor speed gradually decreases in oscillation with an amplitude of [-20; 30] rad, with a period of 3 seconds, starting at 5 rad.
- When decreasing Q6, the tilt angle starts at 0.1 rad and quickly drops to -0.05 rad within 0.5 seconds, then gradually reaches the equilibrium position at 1 second. The disc motor speed oscillates with an amplitude of [-38; 38] rad, with a period of 0.75 seconds, starting at 10 rad.

5. Experiment

5.1. Standard LQR

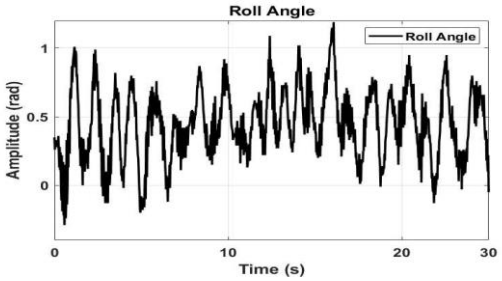

Fig. 21. Stable LQR value for Roll axis

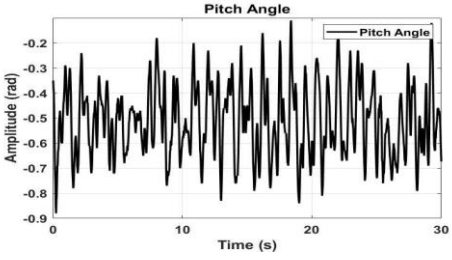

Fig. 22. Stable LQR value for Pitch axis

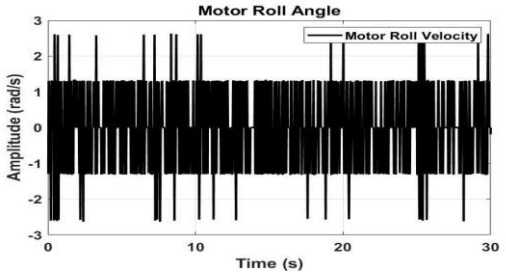

Fig. 23. Output result of the wheel motor velocity

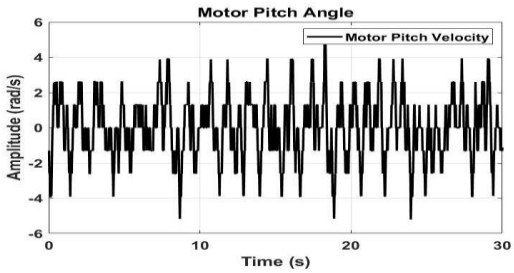

Fig. 24. Output result of the disk motor velocity

Comment: From analyzing the data, it is evident that throughout the 60-second period, both the roll and pitch angles fluctuate around their equilibrium positions. The wheel motor velocity reaches stability at 0 within the first 20 seconds before gradually shifting backward. In contrast, the disk motor velocity demonstrates effective responsiveness, maintaining the robot in an optimal state.

5.2. Change Q_1 value

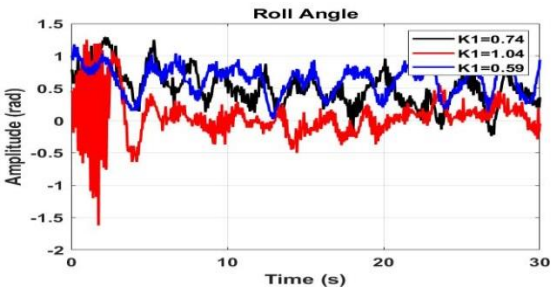

Fig. 25. Modify Q_1 value for Roll axis

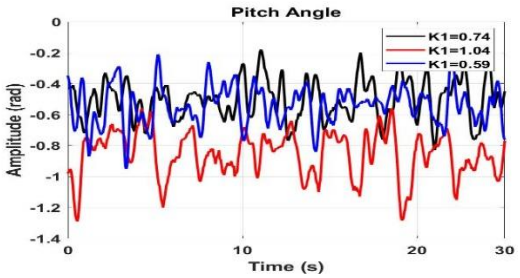

Fig. 26. Modify Q_1 value for Pitch axis

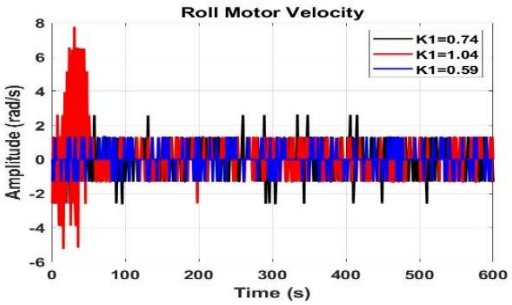

Fig. 27. Output result of the wheel motor velocity

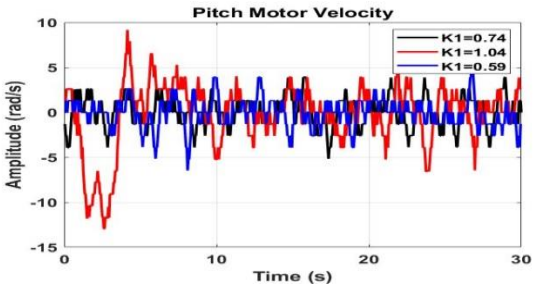

Fig. 28. Output result of the disk motor velocity

Comment:

When Q_1 increases, Fig 25-26 show that the roll angle oscillates around the equilibrium position with a larger amplitude, ranging from [-1.5; 1.5] rad, while the pitch angle tilts significantly during the first 10 seconds before gradually stabilizing, oscillating within [0.25;1] rad. Additionally, Fig 27-28 illustrate that the wheel motor velocity continuously moves up and down, while the disk motor velocity shifts by 0.4 rad.

When Q_1 decreases, Fig 25-26 demonstrate that the control signals for the roll and pitch angles, along with Fig 27-28 showing the wheel and disk motor velocity, oscillate around 0 with a greater amplitude compared to the standard value.

5.3. Change Q_2 value

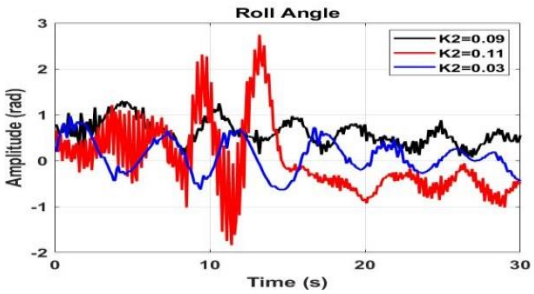

Fig. 29. Modify Q_2 value for Roll axis

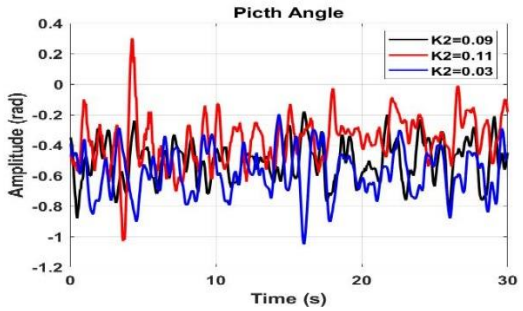

Fig. 30. Modify Q_2 value for Pitch axis

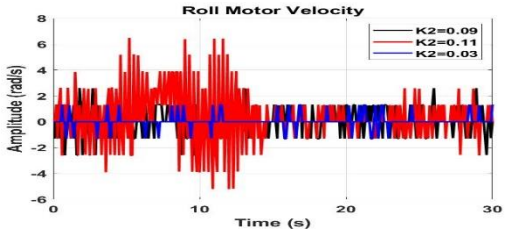

Fig. 31. Output result of the wheel motor velocity

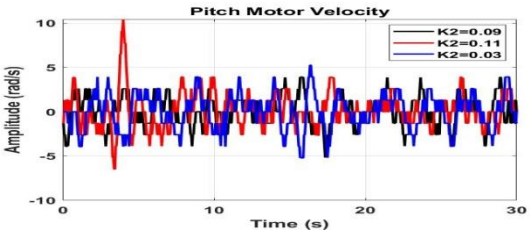

Fig. 32. Output result of the disk motor velocity

Comment:

When Q_2 increases, Fig 29-30 indicate that the roll angle oscillates consistently around the equilibrium position within the range of [-2; 3] rad, while the pitch angle oscillates around -0.6 rad. Additionally, Fig 31-32 show that both the wheel motor velocity and disk motor velocity fluctuate around the equilibrium position.

When Q_2 decreases, Fig 29-30 reveal that the roll and pitch angles oscillate around 0 with a wider range, spanning from [-4; 4] rad and [-0.2; 1] rad, respectively. Fig 31-32 also illustrate that the wheel motor velocity and disk motor velocity continue to oscillate around the equilibrium position.

5.4. Change Q_3 value

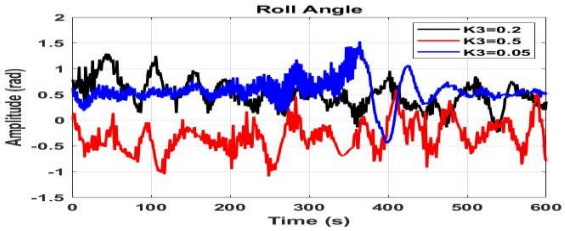

Fig. 33. Modify Q_3 value for Roll axis

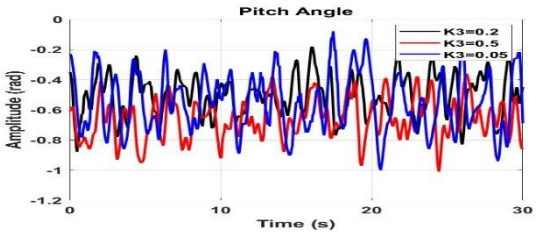

Fig. 34. Modify Q_3 value for Pitch axis

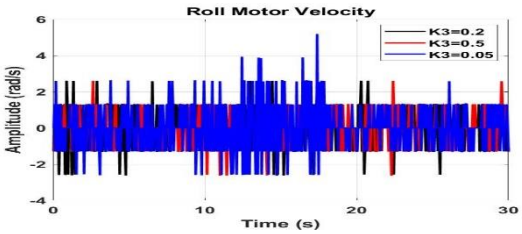

Fig. 35. Output result of the wheel motor velocity

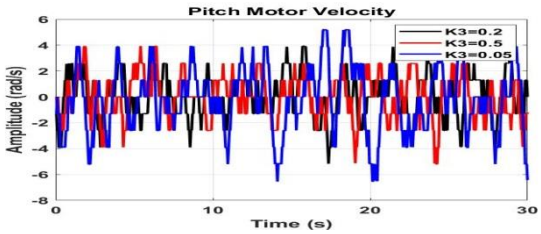

Fig. 36. Output result of the disk motor velocity

Comment:

When Q_3 increases, Fig 33-34 indicate that the roll angle fluctuates around -0.5 rad with an amplitude of 0.5 rad, while the pitch angle oscillates around -0.7 rad. Additionally, Fig 35-36 illustrate that both the wheel motor velocity and the disc motor velocity fluctuate around their equilibrium positions.

When Q_3 decreases, Fig 33-34 show that the roll angle oscillates around 0.5 rad, while the pitch angle fluctuates between [-0.8; -0.2] rad, centering around -0.5 rad. Fig 35-36 also demonstrate that both the wheel motor velocity and the disc motor velocity continue to oscillate around the equilibrium position.

5.5. Change Q_4 value

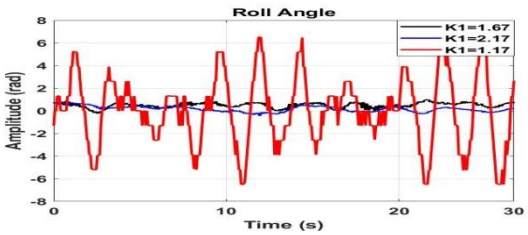

Fig. 37. Modify Q_4 value for Roll axis

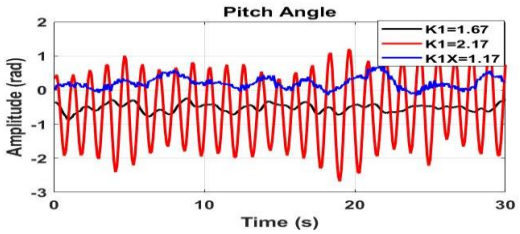

Fig. 38. Modify Q_4 value for Pitch axis

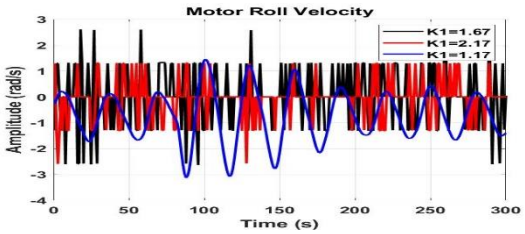

Fig. 39. Output result of the wheel motor velocity

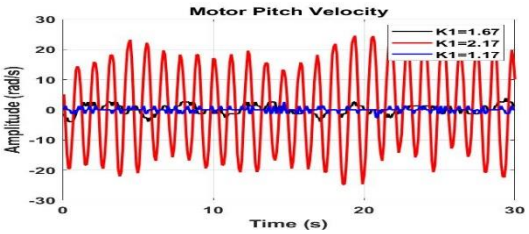

Fig. 40. Output result of the disk motor velocity

Comment:

When Q_4 increases, Fig 37-38 indicate that the roll angle oscillates around 0 rad with a small amplitude, while the pitch angle exhibits more significant fluctuations around 1 rad with an amplitude of 4 rad. Fig 39-40 show that the wheel motor velocity has slight fluctuations around 0 rad, whereas the disc motor velocity oscillates around 0 rad with a relatively larger amplitude.

When Q_4 decreases, Fig 37-38 reveal that the roll angle oscillates around 0 rad with a larger amplitude of about 6 rad, while the pitch angle has smaller fluctuations around 0 rad. Fig 39-40 illustrate that the wheel motor velocity follows a sinusoidal pattern around -0.5, and the disc motor velocity oscillates around 0 rad with a very small amplitude.

5.6. Change Q_5 value

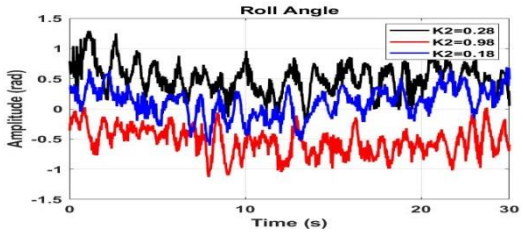

Fig. 41. Modify Q_5 value for Roll axis

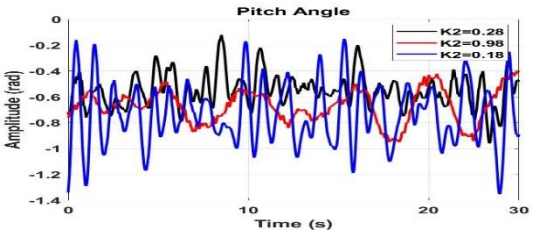

Fig. 42. Modify Q_5 value for Pitch axis

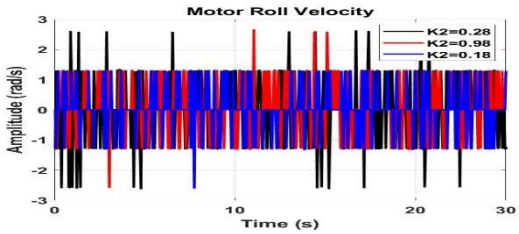

Fig. 43. Output result of the wheel motor velocity

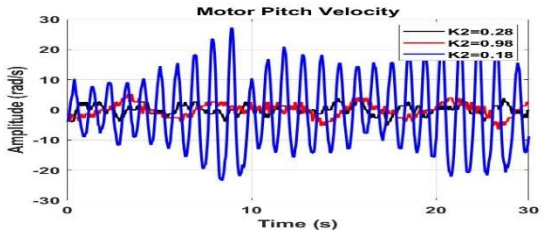

Fig. 44. Output result of the disk motor velocity

Comment:

When Q_5 increases, Fig 41-42 indicate that the roll angle oscillates around -0.5 rad with an amplitude of 0.5 rad, while the pitch angle shows more pronounced oscillations around -0.7 rad with an amplitude of 0.3 rad. Fig 43-44 show that the wheel motor velocity exhibits minor fluctuations around 0 rad, while the disc motor velocity oscillates around 0 rad with a small amplitude.

When Q_5 decreases, Fig 41-42 reveal that the roll angle oscillates around 0.25 rad with a small amplitude, whereas the pitch angle fluctuates around 0.6 rad with a larger amplitude. Fig 43-44 illustrate that the wheel motor velocity oscillates around the equilibrium position, while the disc motor velocity shows fluctuations around 0 rad with a relatively larger amplitude.

5.7. Change Q_6 value

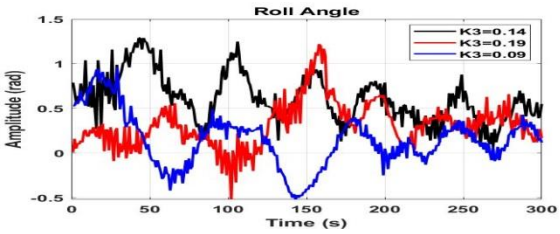

Fig. 45. Modify Q_6 value for Roll axis

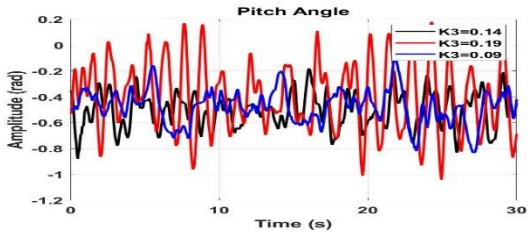

Fig. 46. Modify Q_6 value for Pitch axis

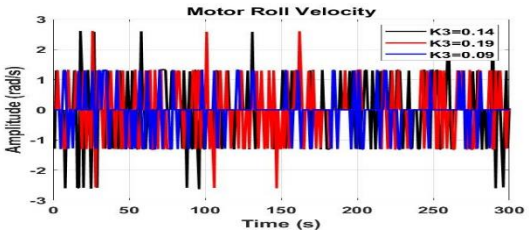

Fig. 47. Output result of the wheel motor velocity

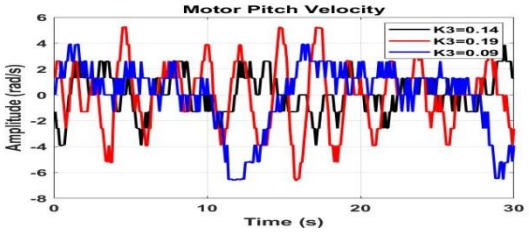

Fig. 48. Output result of the disk motor velocity

Comment:

When Q_6 increases, Fig 45-46 indicate that the roll angle fluctuates irregularly, while the pitch angle oscillates around -0.4 rad. Fig 47-48 show that the wheel motor velocity experiences slight fluctuations around 0, while the disc motor velocity oscillates around 0 rad with a small amplitude.

When Q_6 decreases, Fig 45-46 reveal that the roll angle continues to fluctuate irregularly, but the pitch angle oscillates around -0.64 rad with a small amplitude. Fig 47-48 illustrate that the wheel motor velocity fluctuates around the equilibrium position, while the disc motor velocity oscillates around 0 rad with a relatively larger amplitude.

6. Conclusions

In LQR, the weights in Q and R matrices are critical in shaping the control system's performance. The Q matrix prioritizes the system's state variables, while the R matrix emphasizes the control input signals. Changes in these weights shift the balance between state accuracy and control cost.

An increase in Q matrix values signified a greater focus on state precision, leading to stronger control but possibly higher energy or resource consumption. In contrast, increasing the R matrix values reduced control signal usage, making control more efficient but potentially sacrificing accuracy or slowing the system's response. Striking the right balance is essential for optimal system performance, depending on the specific control requirements.

Acknowledgement

This paper belongs to project for students of Ho Chi Minh City of Technology and Education (HCMUTE) in year 2025. It is funded by HCMUTE. We also want to give thanks to PhD. Van-Dong-Hai Nguyen due to helping us operating the experimental model.

7. References:

[1] Schoonwinkel A.: "Design and test of a computer stabilized unicycle", Ph.D. dissertation, Stanford Univ., Stanford, CA, 1987.

[2] Sheng Z., Yamafuji K.: "Postural stability of a human riding a unicycle and its emulation by a robot", IEEE Trans. Robot. Autom., vol. 13, no. 5, pp. 709–720, 1997.

[3] Lee J.-H. et al: "Novel air blowing control for balancing a unicycle robot", in Proc. IEEE/RSJ Int. Conf. Intell. Robots Syst., pp. 2529–2530, 2010.

[4] Lee J. et al: "Decoupled Dynamic Control for Pitch and Roll Axes of the Unicycle Robot", IEEE transactions on industrial electronics, vol. 60, no. 9, 2013.

[5] Han S.I., Lee J.: "Balancing and Velocity Control of a Unicycle Robot Based on the Dynamic Model", IEEE Transactions on Industrial Electronics 62, pp. 405-413, 2015.

[6] Shen J, Hong D.: "OmBURo: A Novel Unicycle Robot with Active Omnidirectional Wheel", IEEE International Conference on Robotics and Automation (ICRA), pp. 8237-8243, 2020.

[7] NXTway-GS (self-balancing two-wheeled robot) controllerdesign, LEGOMindstorm, Enfield, CT, Tech.Rep[Online].Available:http://www.mathworks.com/matlabcentral/fileexchange/19147.

[8] Dorf R.C., Bishop R.H.: „Modern Control System, 10th Edition: Optimal Control System", Upper Saddle River, NJ: Pearson, 2005.

[9] Tanaka Y., Murakami T.: "A study on straight-line tracking and posturecontrol in electric bicycle", IEEE Trans. Ind. Electron., vol. 56, no. 1, pp. 159–168, 2009.

[10] Vu D.H: et al: "A Survey of Linear Control for Unicycle Robot", Robotica & Management, Vol. 29, No. 1, pp. 45-54, 2024.